



Sextos, A., Faraonis, P., Zabel, V., Wuttke, F., Arndt, T., & Panetsos, P. (2016). Soil-Bridge System Stiffness Identification through Field and Laboratory Measurements. *Journal of Bridge Engineering*, 21(10), [04016062]. [https://doi.org/10.1061/\(ASCE\)BE.1943-5592.0000917](https://doi.org/10.1061/(ASCE)BE.1943-5592.0000917)

Peer reviewed version

Link to published version (if available):
[10.1061/\(ASCE\)BE.1943-5592.0000917](https://doi.org/10.1061/(ASCE)BE.1943-5592.0000917)

[Link to publication record in Explore Bristol Research](#)
PDF-document

This is the author accepted manuscript (AAM). The final published version (version of record) is available online via ASCE at [http://ascelibrary.org/doi/abs/10.1061/\(ASCE\)BE.1943-5592.0000917](http://ascelibrary.org/doi/abs/10.1061/(ASCE)BE.1943-5592.0000917). Please refer to any applicable terms of use of the publisher.

University of Bristol - Explore Bristol Research

General rights

This document is made available in accordance with publisher policies. Please cite only the published version using the reference above. Full terms of use are available: <http://www.bristol.ac.uk/red/research-policy/pure/user-guides/ebr-terms/>

Soil-bridge system stiffness identification through field and laboratory measurements

Anastasios Sextos¹ Member ASCE, Periklis Faraonis², Volkmar Zabel³,
Frank Wuttke⁴, Tobias Arndt⁵, Panagiotis Panetsos⁶

Abstract

Despite the major advances in finite element (FE) modeling and system identification (SI) of extended infrastructures, soil compliance and damping at the soil-foundation interface are not often accurately accounted for due to the associated computational demand and the inherent uncertainty in defining the dynamic stiffness. This paper aims to scrutinize the effect of soil conditions in the SI process and to investigate the efficiency of advanced FE modeling in representing the superstructure-soil-foundation stiffness. For this purpose, use is made of the measured, computed and experimentally identified natural frequencies of a real bridge. Field measurements that were obtained during construction were reproduced both in the laboratory and by refined FE modeling. In addition, to understand the physical problem more thoroughly, three alternative soil conditions were examined, namely, rock, stabilized soil and Hostun sand. Discrepancies in the order of 3-13% were observed between the identified and the numerically predicted natural frequencies. These discrepancies highlight the importance of reliable

¹ Associate Professor, Department of Civil Engineering, Aristotle University of Thessaloniki, Greece, e-mail: asextos@civil.auth.gr & Department of Civil Engineering, University of Bristol, UK, email: asextos@bristol.ac.uk

² MSc., Phd student, Department of Civil Engineering, Aristotle University of Thessaloniki, Greece, e-mail: pfaraonis@civil.auth.gr

³ Dr.-Ing., Bauhaus University of Weimar, Marienstrasse 15, 99423 Weimar, Germany, e-mail: volkmar.zabel@uni-weimar.de

⁴ Professor, Chair of Marine and Land Geomechanics & Geotechnics, Kiel University, Ludewig-Meyn Street 10, 24118 Kiel, Germany, e-mail: fw@gpi.uni-kiel.de (before Bauhaus-University Weimar / Geomechanics)

⁵ MSc., PhD student, Bauhaus University of Weimar, Coudraystrasse 11c, 99423 Weimar, Germany, e-mail: tobias.arndt@uni-weimar.de

⁶ Dr. Civil Engineer, Capital Maintenance Department, Egnatia Odos S.A., 60km Thessaloniki-Thermi, 57001 Thermi, ppane@egnatia.gr

19 estimation of soil properties and compliance with the SI framework for extended bridges under
20 ambient and low amplitude vibrations.

21 **Introduction**

22 It has long been shown through scientific research worldwide that structural engineering projects
23 should not be designed without considering the effect of soil conditions, especially in the case
24 of structures of major significance or those resting on soft and/or varying soil profiles (see
25 Sextos, 2014 for a summary). The most comprehensive way of accounting for soil stiffness is
26 to study the structure-foundation-soil system as a whole (Wolf, 1989). However, due to the high
27 computational demand associated with FE modelling, alternative methods have been developed.
28 These methods involve kinematic and inertial decoupling through the appropriate modeling of
29 dynamic stiffness for different foundation shapes (circular, rectangular, arbitrary), embedment
30 depths (surface, shallow embedded, intermediate embedded, pile) and foundation subsoils (deep
31 uniform deposit, multi-layer deposit, shallow stratum over rock) (Veletsos and Wei, 1971;
32 Dominguez and Roesset, 1978; Wong and Luco, 1985; Kausel, 1974; Gazetas et al., 1985).
33 In particular, shallow embedded circular foundations and caissons (i.e., with a length-to-
34 diameter aspect ratio, $D/B < 2$) are commonly modeled by replacing the foundation-soil system
35 with six degrees of freedom (6 DOF) springs, the stiffness of which is typically calculated
36 according to Elsabee and Morray (1977) and Gazetas et al. (1985). Alternatively, shallow
37 embedded foundations are also treated as intermediate embedded foundations (with a length-to-
38 diameter aspect ratio, $2 < D/B < 6$). Based on this approach, the subsoil may be replaced by 6-
39 DOF springs lumped at the base of the foundation (Kausel, 1974; Kausel & Ushijima, 1979),
40 while additional 6-DOF springs are attached at the middle of the foundation height (Gerolymos
41 and Gazetas, 2006; and improved by Varun et al., 2009).
42 Notwithstanding the major advances made in quantifying the stiffness of the soil-bridge system,
43 the reliable validation of the above spring coefficients remains an open issue with a significant

44 impact for the safety of bridge engineering projects. The majority of experimental work
45 conducted along these lines consists of laboratory testing of specific foundation-soil
46 components, tested either on a shaking table or in a centrifuge, as well as entire scaled bridge-
47 foundation-soil systems without the superstructure (Finn, 2005). Based on the responses
48 measured in the laboratory, various constitutive laws and numerical predictions of soil stiffness
49 have been compared, verified and/or optimized.

50 Alternatively, implicit on-site evidence regarding the effect of soil-structure interaction on the
51 dynamic and seismic responses of bridges has also been provided by means of SI, for example,
52 on real bridges (Crouse et al., 1987; Chaudhary et al., 2001; Todorovska, 2009;) on a bridge
53 replica at a test site (Manos et al., 2014) and on buildings (Stewart et al., 1998; Taciroglou et
54 al., 2014; Shamsabadi et al., 2016). SI is an advanced tool for the inverse prediction of the
55 dynamic characteristics (i.e. natural frequency, damping ratio and mode shape) of structures that
56 also accounts for the inherent properties of the supporting soil. The results of SI are usually
57 exploited to validate the developed finite element models by comparing and ultimately matching
58 the identified and the numerically predicted dynamic characteristics of a structure. Critical
59 reviews, qualitative and quantitative comparisons among alternative SI methods based on
60 benchmark structures, as well as their recent developments are expounded in the literature
61 (Andersen et al., 1999; Peeters and De Rock, 2001; Peeters and Ventura, 2003; Antonacci et al.,
62 2012; Reynders, 2012).

63 Based on the above, it is clear that the impact of soil-structure interaction on the dynamic
64 response of a bridge-foundation-soil system is most commonly validated either in the laboratory,
65 with controlled soil conditions but subject to the inevitable limitations of scaling, or on-site, that
66 is, in real scale but without laboratory-controlled soil conditions or the potential to study the
67 relative effects of different soil stiffnesses. These limitations hinder the appraisal of existing
68 analytical solutions and numerical approaches for considering soil stiffness under both realistic

69 scale and soil conditions. Along these lines, the scope of this paper is to study the implications
70 of soil-structure interaction on the modal identification of a real bridge-soil system by making
71 use of measurements obtained at both the macro (prototype) and the laboratory scales, and by
72 utilizing in-situ ambient vibrations and artificially produced ambient loads, respectively. The
73 above comparison enables (a) the validation of different, widely used modeling approaches and
74 spring constants against measured data, and subsequently (b) the comparative assessment of the
75 impact of alternative soil conditions on the extracted modal parameters of the soil-structure
76 interacting system.

77 The case studied herein is a segment of the (527 m long) Metsovo bridge in Greece. Ambient
78 vibration measurements were obtained at the level of the deck at the construction stage (Panetsos
79 et al., 2010) during which the partially constructed bridge was responding as a T-shaped
80 cantilever. The apparent advantage of this particular case is that at the time of construction the
81 (single, at this stage) M_3 pier-deck segment consisted of a simple and easy-to-model-and-test
82 structural system (Figure 1). In addition, its stiff foundation soil facilitated the construction of a
83 dynamically equivalent system at the laboratory, because the uncertainty associated with the soil
84 conditions was relatively minor (Figure 2). The latter equivalent system had been studied under
85 similar (rock) conditions at the laboratory before its response was extrapolated for the case of
86 alternative soil conditions (i.e., stabilized soil and Hostun sand). The laboratory and the on-site
87 identification campaigns, as well as the development of alternative numerical models and the
88 subsequent quantification of their associated model qualities are presented in the following
89 sections. A synopsis of this work that focuses exclusively on a single type of soil can also be
90 found elsewhere (Faraonis et al., 2014).

91 **Prototype structure**

92 *Description of the structural system*

93 The Metsovo ravine bridge was constructed in 2008 in Greece along the 650 km Egnatia

94 Highway. The bridge was constructed with the balanced cantilever construction method, which
95 made feasible the modal identification of structurally independent T-shaped cantilever bridge
96 segments during construction. The modal characteristics of pier M_3 and the respective deck
97 segment (Figure 1) were identified by Panetsos et al. (2010) prior to the construction of the key
98 section, which connected the segment to the M_2 pier-deck (that acted as a temporary, balanced
99 cantilever). At the time the measurements were obtained, the total length of the deck temporarily
100 supported by the M_3 cantilever was 215 m, while the height of the pier itself was 32 m. The pier
101 was founded with a large caisson in subsoil characterized by thickly bedded interchanges of
102 sandstones and limestones. More specifically, the subsoil mechanical properties have been
103 defined as follows: i) vertical and horizontal friction angle, $\phi_v=25^\circ$ and $\phi_h=35^\circ$ (based on shear
104 strength laboratory tests), ii) vertical and horizontal cohesion, $c_v=100 \text{ kN/m}^2$ and $c_h=100 \text{ kN/m}^2$
105 (also based on the same set of tests), iii) unconfined compression strength, $q_u=15 \text{ MPa}$ (based
106 on unconfined compressive strength laboratory tests) and iv) one-dimensional confined
107 compression modulus, $E_{o,static}=1/mv=400\text{-}1000 \text{ MPa}$ (based on Menrad Pressuremeter field
108 tests). Furthermore, Lugeon field tests depicted no evidence of a permanent underwater aquifer
109 in the vicinity of the bridge. Column 1 of Table 1 summarizes the section and material properties
110 of the prototype structure (referred to as “actual structure” hereafter for the purposes of
111 comparison with the laboratory models).

112 *System identification of the prototype structure*

113 The modal identification of the M_3 cantilever was based on ambient vibration measurements
114 triggered by wind and operational loads. Five frequencies were successfully identified, in the
115 range of 0.159-0.908 Hz, as shown in Table 2; column 1 of the table corresponds to one
116 rotational, two longitudinal, one transverse and one bending mode of vibration. Detailed
117 information regarding the measurements, the accelerometer installation configuration and the
118 applied identification methodology can also be found in Panetsos et al. (2010).

119

Fixed scaled structure

120 *Scaling laws & dimensional analysis*

121 The construction of a scaled structure primarily determines the scaling laws relating the material
122 and geometry of the prototype to those of the scaled structure. These scaling laws can be
123 determined either by dimensional analysis or the analysis of the system's characteristic equation.
124 Based on dimensional analysis and by neglecting the gravity distortion effects that inevitably
125 arise during scaling, the scaling factor that relates the natural frequencies of a scaled structure
126 with its prototype can be taken as (Bridgman, 1931):

$$\lambda_f = \frac{1}{\lambda_l} \cdot \sqrt{\frac{\lambda_E}{\lambda_\rho}} \quad (1)$$

127 where: λ_f is the prototype to the model frequency ratio,

128 λ_l is the prototype to the model dimension ratio,

129 λ_E is the prototype to the model Young's modulus of elasticity ratio,

130 λ_ρ is the prototype to the model density ratio.

131 Based on Equation 1, it is evident that if the construction of a scaled structure that is identical
132 to the prototype was indeed feasible at a 1:100 scale ($\lambda_l=100$) using the same materials is the
133 actual structure ($\lambda_E=1$ and $\lambda_\rho=1$), then the prototype to the model frequency ratio would be equal
134 to $\lambda_f=1/100$. In such a case, this theoretically scaled model would have the section and material
135 properties presented in column 2 of Table 1, and its natural frequencies would vary between
136 15.90 and 90.80 Hz, as also shown in the same column. These (ideally, acquired) natural
137 frequencies are therefore deemed in this study as the *target* dynamic properties of the fixed
138 scaled model constructed in the laboratory.

139 *Construction of the fixed scaled structure*

140 Given the long deck of the T-shaped prototype cantilever (which was extended to 215 m as seen
141 in Figure 1) and the limited space available in the laboratory, the scale of the equivalent structure

142 was set to 1:100. This particular scale did not enable the construction of an exact replica of the
143 concrete deck section, because this would have resulted in web and flange dimensions as thin
144 as 22 mm and 3 mm, which are impossible to cast. As a result, an equivalent steel structure was
145 designed to represent the same dynamic characteristics as the ideally scaled structure, after
146 appropriate optimization of the dimensions were made to match those of standard sections that
147 were available in the market. The optimization of the equivalent section dimensions was
148 performed numerically using the FEA software ABAQUS 6.12. The model was fixed at its base
149 in order to represent the stiff foundation soil of the actual conditions of the prototype structure.
150 The above procedure resulted in an equivalent steel balanced cantilever, which was assembled
151 using the following commercially available sections (Figure 2):

- 152 • a 90×90×3 HSS hollow steel section of 215 cm length corresponding to a 1:100 replication
153 of the prototype deck,
- 154 • a 100×100×5 HSS hollow steel section of 6.15 cm length corresponding to a 1:100 replication
155 prototype of the central deck-segment,
- 156 • two 80×20×3 HSS hollow steel sections of 32 cm length corresponding to a 1:100 replication
157 of the prototype, twin blade, M₃ pier, and
- 158 • a 100×100×5 steel plate, which was used as the base of the pier. Four holes enabled the above
159 steel sections to be bolted and fixed to a laboratory shaking table. These holes were also used
160 later to bolt the pier deck system to the caisson embedded into the soil.

161 The section and material properties of the fixed scaled structure are summarized in column 3 of
162 Table 1.

163 ***Stochastic subspace identification***

164 To identify the natural frequencies, mode shapes and damping ratios of the fixed scaled
165 structure, an output-only ambient vibration-based SI process was applied involving the
166 covariance-driven stochastic subspace identification method available in the MACEC Matlab

167 toolbox (Reynders & De Roeck, 2007). More information regarding this method can be found
168 in Van Overschee and De Moor (1996) and Peeters and De Roeck (1999). A hammer was used
169 to excite the structure at the deck level, thus resembling the broadband nature of the actual
170 ambient vibration of the actual structure. It should be noted that this broadband type excitation
171 is consistent with the utilized modal identification method adopted; however, it is not intended
172 to be used for non-stationary excitations (i.e., for seismic assessment purposes).

173 *System identification of the fixed scaled structure*

174 The scaled structure was constructed in the Soil Mechanics laboratory at the Bauhaus University
175 Weimar, in Germany, and was fixed initially on the base of the shaking table. This particular
176 “baby” shaking table has dimensions $1 \times 1 \text{ m}^2$ and is capable of imposing 35 mm displacements
177 within the frequency range of 2.5-30 Hz. Six triaxial accelerometers placed along the
178 longitudinal, transverse and vertical directions were installed on the structure. Five of those were
179 set up on the deck and one at the base of the pier. Three of the above six sensors, namely RS₁,
180 RS₂ and RS₃, were considered as the reference sensors (RS) and thus remained steady. Sensors
181 S₄-S₆ were placed in three alternative configurations (C1, C2 and C3; Figure 3). All
182 accelerometers were of the same type (Model 356A16 by PCB Piezotronics Inc): weight 7.4 g,
183 frequency range 0.3-6000 Hz and sensitivity 10.2 mV/(m/sec²).

184 The first five identified natural frequencies (Figure 4) of the fixed scaled structure were found
185 to correspond to the following mode shapes (listed in order of identification): rotational around
186 the pier axis (1st), longitudinal along the deck axis (2nd), closely spaced coupled longitudinal and
187 transverse (3rd and 4th) and bending (5th). Based on the field measurements, these laboratory-
188 identified mode shapes matched the sequence of the first five eigenmodes identified for the
189 actual (real scale) M₃ pier cantilever, with the exception of the two coupled modes (i.e., the 3rd
190 and the 4th mode of the actual structure, which were identified as uncoupled transverse and
191 uncoupled longitudinal, respectively). From column 3 of Table 2, it can also be observed that

192 the natural frequencies of the steel, fixed scaled structure ranged between 15.87 and 88.99 Hz.
193 This matched very well to the target frequencies of the ideal (i.e., the theoretical, concrete model
194 scaled to 1:100) structure, as they presented a mere 6.74% average deviation (see Table 2 for
195 deviation definition). This qualitative (in terms of mode shapes and order) and quantitative (in
196 terms of natural frequencies) agreement between the equivalent fixed scaled and the idealized
197 scaled structures was deemed satisfactory and hence, the equivalent steel model was considered
198 reliable enough for the envisaged comparative study.

199 **Scaled structure embedded in soil**

200 Having established a level of confidence regarding the equivalence of the scaled structure to the
201 prototype, additional measurements were performed for two alternative soil types of decreasing
202 stiffness, namely for stabilized soil and Hostun sand.

203 ***Stabilized soil***

204 A soil can be characterized as stabilized when its stiffness has been increased by lime injection.
205 According to the grain size distribution curve presented in Figure 5 (left), the particular soil used
206 consisted of 75% clay, 10% sand and 15% gravel. Its liquid limit (LL) was equal to 42, and
207 more than 50% of the grain passed the #200 sieve. Based on the above information and the
208 ASTM D2487 (2011) guidelines, the soil was characterized as “gravelly lean clay”. The required
209 percentage of added lime was determined to be 4% according to DIN EN 459-1 (2010)
210 standards. Based on a standard Proctor compaction test, the optimal water content was
211 determined to be 24% and the maximum achieved dry density of the mix was equal to
212 $\rho_s=1.86\text{t/m}^3$.

213 The stabilized soil was placed in six layers of 5 cm height each, within a laboratory box of 95
214 cm diameter and 40 cm height that was fixed on the shaking table (Figure 6a). For each layer,
215 soil and water were initially mixed at the laboratory mixture machine (Figure 6b) before lime
216 was injected (Figure 6c). Next, each layer was placed inside the laboratory box and was

217 compacted by a laboratory compaction tool until it reached the target 5 cm height (Figure 6d).
218 The final surface of every layer was manually coarsened with the use of a knife to enhance the
219 cohesion with the overlying layer (Figure 6e). Eventually, the scaled structure was fixed
220 (essentially bolted) on a 15 cm diameter circular concrete foundation of class C30/37 Eurocode
221 8 (compressive strength, $f_{ck}=30$ MPa) resembling the caisson of the actual structure, which was
222 embedded in the upper three layers of the stabilized soil (Figures 6f and 7).
223 Four sensors were placed inside the box: two measuring the shear wave velocity (V_S) and two
224 measuring the compression wave velocity (V_P) of the stabilized soil. The V_S sensors had a 17
225 cm separation distance and were placed at a 15 cm height, corresponding to the same level where
226 the base of the concrete foundation was placed inside the box. The V_P sensors were placed 5 cm
227 below the V_S sensors at 19.5 cm apart. Due to the reaction of lime with the clay, daily
228 measurements were conducted for 28 consecutive days in order to capture the evolution of the
229 stabilized soil stiffness with time. It is noted, however, that in a preliminary work (Faraonis et
230 al., 2014), the measured values of V_S did not fully match those predicted by the numerically-
231 based SI. Therefore, a detailed investigation was undertaken to re-assess soil properties for the
232 28-day measurements. More specifically, the V_P measurements were utilized to back-assess the
233 V_S based on Equation 2, by assuming a realistic value for the Poisson's ratio of the stabilized
234 soil ($\nu = 0.35$). Based on this investigation, the V_P measurement of the 14th day (345 m/sec) was
235 used for the numerical model as a representative value of the stabilized soil stiffness; hence,
236 leading to a V_S value of (166 m/sec), through:

$$V_S = \sqrt{\frac{V_P^2 - 2\nu V_P^2}{2(1-\nu)}} \quad (2)$$

237 The shear modulus, G , was then determined to be 51 MPa (for $V_S=166$ m/s and $\rho_s= 1.86$ t/m³),
238 according to:

$$G = V_s^2 \rho \quad (3)$$

239 ***Hostun sand***

240 In the last case study, the stabilized soil was removed from the laboratory box and replaced by
241 Hostun sand (Figure 8). The Hostun sand was dry and loose with a friction angle $\phi=35^\circ$,
242 cohesion $c=0$ kPa and relative density $Dr(\%) = 50$. The total height of the Hostun sand in the
243 box was 35.5cm and its dry density was measured as $\rho_s=1.33$ t/m³. The grain size distribution
244 curve of the Hostun sand is presented in Figure 5 (right curve). The scaled structure was also
245 fixed at the circular concrete foundation of 15 cm diameter and height, which was similarly
246 embedded in the upper 15 cm of the sand. The G of the Hostun sand was determined to equal
247 4.6 MPa ($V_p=96$ m/sec, $\nu=0.20$, $V_s=59$ m/s and $\rho_s= 1.33$ t/m³) based on a procedure similar to
248 the one described for the stabilized soil.

249 ***System identification of the equivalent scaled structure embedded in the two examined soils***

250 In both soil cases studied, the structure was excited at the deck level by hammer impact loads.
251 The dynamic characteristics of the bridge model structure were then identified based on the
252 same method (i.e., covariance-driven stochastic subspace identification) used for the fixed
253 scaled model. Identical accelerometer arrangements were also employed.

254 The first five natural frequencies and mode shapes identified at the scaled structure that was
255 founded on stabilized soil ranged between 14.88 and 85.04 Hz, and are presented in column 5
256 of Table 2 and Figure 9a. Compared with those identified for the fixed-base structure, these
257 identified frequencies were reduced by 4-30% depending on the way in which different modes
258 had been affected by soil compliance. More precisely, the natural frequencies of the bending
259 and rotational modes were reduced by 4% and 6%, respectively, while the natural frequencies
260 of the transverse and the two longitudinal modes, which were directly affected by soil flexibility,
261 were reduced by 15% to 30%. On the other hand, the identified damping ratios at the bridge-

262 foundation-stabilized soil system ranged between 0.37% and 3.27%, confirming an increase
263 compared to the damping ratios identified for the fixed bridge-foundation system (0.12-0.57%),
264 as shown in columns 5 and 3 of Table 2, respectively.

265 For the case of the Hostun sand, a further decrease of 19-76% was observed in the identified
266 natural frequencies, which were found to vary between 9.60 Hz and 71.85 Hz (Table 2, column
267 9). A corresponding increase was also observed in the identified damping ratios (1.27-8.59%)
268 compared to the case of the stabilized soil, as seen in column 9 of Table 2. No difference was
269 observed in the sequence of the first five identified modeshapes, illustrated in Figure 10a.

270 The decreases in the identified natural frequencies and in the amplification of the identified
271 damping ratios are attributed to the gradually decreasing stiffness of the bridge-foundation
272 system (i.e., shifting from fixed to stabilized soil and then to Hostun sand). As anticipated, even
273 for ambient vibrations, soil stiffness played a significant role in the identified dynamic
274 characteristics of the structure, particularly for translational modes related to vibration along the
275 longitudinal and the transverse axes of the bridge. Assuming, for illustration purposes, that the
276 fixed boundary conditions correspond to a rock condition with a shear wave velocity of 800 m/s,
277 Figure 11 illustrates the above experimentally-verified influence of decreasing soil stiffness on
278 the identified natural frequencies of the scaled bridge structure.

279 **Numerical modeling**

280 In order to investigate the efficiency of existing numerical methods and analytical expressions
281 in simulating the soil stiffness, alternative FE models were developed for the three scaled soil-
282 foundation-pier systems (namely, fixed, stabilized soil and Hostun sand).

283 ***Fixed pier base***

284 Initially, a refined FE model was developed using three-dimensional (3D) solid elements to
285 simulate the fixed scaled structure (Table 1, column 4). The FE model consisted of
286 approximately 19,000 triangular brick elements with 88,620 DOF. The measured mass of the

287 physical model was 20.46 kg with a density of $\rho=7.46 \text{ t/m}^3$, while the modulus of elasticity of
288 the stainless steel was 210 GPa.

289 The efficiency of the fixed numerical model in predicting the mode shapes of the constructed
290 fixed scaled structure was assessed by the modal assurance criterion (MAC), which compares
291 vectors of the identified mode shapes with those calculated by a numerical model, essentially
292 through the squared correlation between two modal vectors (Allemang & Brown, 1982):

$$|MAC(\phi_i, \phi_j)| = \left| \frac{\phi_i^T \times \phi_j}{\|\phi_i\| \times \|\phi_j\|} \right| \quad (4)$$

293 where, ϕ_i is the measured vector of the $i^{\text{th}} = \{1, \dots, n\}$ mode shape and ϕ_j is the calculated vector
294 of the $j^{\text{th}} = \{1, \dots, n\}$ mode shape. By definition, the index of the MAC ranges between 0 and 1;
295 the closer the MAC value is to unity, the closer the fit between the measured and the
296 numerically-predicted mode shapes.

297 ***Compliant pier base***

298 For the two cases where the scaled structure was fixed on a circular concrete foundation and
299 embedded into stabilized soil or Hostun sand layers, the pier-foundation-subsoil system was
300 modeled using three alternative approaches.

301 ***Direct method model***

302 The dynamic stiffness of the soil was first simulated in the 3D space using solid finite elements
303 of approximately 180,000 DOF (Table 1, columns 6 and 10). The G of the stabilized soil was
304 51 MPa (section 4.1) and the Poisson's ratio was assumed to be $\nu=0.35$. For the case of the
305 Hostun sand, G was set to 4.6 MPa (section 4.2) and its Poisson's ratio was assumed to be
306 $\nu=0.20$. The same superstructure sections were assumed as for the fixed scaled model, with the
307 properties of stainless steel equal to $E=210 \text{ GPa}$ and $\nu=0.30$ along with a C30/37 class concrete

308 material with $E=32$ GPa and $\nu=0.30$ for caisson modeling. The mass of the foundation was
309 measured as 7.56 kg corresponding to a density $\rho=2.71$ t/m³.

310 *Intermediate embedded circular foundation model*

311 A second approach to model the foundation-soil system (Table 1, columns 7 and 11) was based
312 on the formulas proposed for intermediate embedded circular foundations (for a length-to-
313 diameter aspect ratio, $2 < D/B < 6$). In this case, the superstructure and the foundation were
314 simulated in the same manner as in the first direct approach but springs were employed instead
315 of a 3D soil volume. In particular, the subsoil at the tip of the caisson was modeled as a 6-DOF
316 spring, while the lateral stiffness of the surrounding soil was modeled by an additional 6-DOF
317 spring assigned at the middle of the foundation height. Both 6-DOF stiffness matrices were
318 obtained from the long established theory of surface circular foundations on a stratum over a
319 rigid base as suggested by Kausel (1974) and Kausel and Ushijima (1979) and the solution of
320 Varun et al. (2009) for cylindrically shaped intermediate embedded foundations, respectively
321 (Table 3).

322 The resulting stiffness terms were derived for the stabilized soil ($G=51$ MPa, $\nu=0.35$) equal to
323 $\{K_{h,x}, K_{h,y}, K_v, K_{r,x}, K_{r,y}, K_t\} = \{23297$ kN/m, 23297 kN/m, 38796 kN/m, 96 kNm/rad, 96
324 kNm/rad, 115k Nm/rad} for the tip and $\{37946$ kN/m, 37496 kN/m, 41767 kN/m, 622 kNm/rad,
325 622 kNm/rad, 615 kNm/rad} for the lateral resistance. For the case of the Hostun sand ($G=4.6$
326 MPa, $\nu=0.20$), the stiffness terms of the tip and lateral 6-DOF matrices were $\{1915$ kN/m, 1919
327 kN/m, 2826 kN/m, 7 kNm/rad, 7 kNm/rad, 10 kNm/rad} and $\{3024$ kN/m, 3024 kN/m, 3480
328 kN/m, 49 kNm/rad, 49 kNm/rad, 55 kNm/rad }, respectively. Notably, these values are small as
329 a result of the small dimensions of the tested model.

330 *Shallow embedded cylindrical foundation model*

331 In the third approach (Table 1, columns 8 and 12), the superstructure and the foundation were

332 again simulated in the same manner as in the first approach, but the soil was replaced by a single
333 set of 6-DOF Winkler type springs, which were placed in the middle of the foundation height.
334 Their values were obtained according to the theory of shallow embedded cylindrical foundations
335 (of a length-to-diameter aspect ratio, $D/B < 2$) resting on a homogenous soil stratum over
336 bedrock, as proposed by Elsabee and Morray (1977) and Gazetas et al. (1985) (Table 3).
337 The stiffness terms for the case of the stabilized soil ($G=51$ MPa, $\nu=0.35$) were derived equal to
338 $\{K_{h,x}, K_{h,y}, K_v, K_{r,x}, K_{r,y}, K_t\} = \{79503 \text{ kN/m}, 79503 \text{ kN/m}, 80563 \text{ kN/m}, 623 \text{ kNm/rad}, 623$
339 $\text{kNm/rad}, 731 \text{ kNm/rad}\}$ and $\{6040 \text{ kN/m}, 6040 \text{ kN/m}, 6307 \text{ kN/m}, 43 \text{ kNm/rad}, 43 \text{ kNm/rad},$
340 $65 \text{ kNm/rad}\}$ for the case of the Hostun sand ($G=4.6$ MPa and $\nu=0.20$).

341 **Comparative assessment of the identified and the numerically-predicted natural** 342 **frequencies of the tested bridge pier-caisson-soil system**

343 ***Fixed pier base***

344 Following the identification of the natural frequencies of the fixed base and the two compliant
345 bridge pier-caisson-soil systems, the efficiencies of the developed numerical models to capture
346 the measured dynamic characteristics were studied carefully, starting from the simpler, fixed-
347 base support conditions. It was indeed verified that the first five natural frequencies predicted
348 by the fixed FE model ranged between 16.02 and 89.46 Hz, thus being in very good agreement
349 with those of the fixed structure tested in the laboratory, and which showed a minor average
350 error of 2.12% as summarized in column 4 of Table 2. A visual comparison between the
351 identified and the numerically-predicted mode shapes for the case of the fixed structure is also
352 provided in Figure 4, while a more accurate comparison is illustrated through the MAC values
353 in Figure 12. It is shown that the 1st (rotational), 2nd (1st longitudinal) and 5th (bending) modes
354 of vibration matched very satisfactorily, with MAC values close to 1. On the other hand, the
355 numerically-predicted 3rd (transverse) and 4th (2nd longitudinal) modes did not match as
356 successfully (i.e., MAC values 0.68 and 0.60, respectively). This fact is mainly attributed to the

357 low excitation of the identified 3rd and 4th modes and to the applied fixed boundary conditions
358 that resulted in the close spacing of these modes (i.e., 65.31 and 66.74 Hz) thus hindering their
359 distinction. As shown in Figures 9 and 10, this limitation is raised for the cases of the stabilized
360 soil and the Hostun sand, where the identified 3rd and 4th modes were not closely spaced and
361 thus they could easily be distinguished.

362 ***Compliant pier base***

363 Next, the efficiency of the three alternative numerical methods described above was compared
364 in order to predict the dynamic characteristics of the soil-compliant system tested in the
365 laboratory. For the case that simulated the stabilized soil with the direct method model (3D FEs,
366 section 5.2.1) as an intermediate embedded foundation (6+6-DOF springs, section 5.2.2), or as
367 a shallow embedded foundation (6-DOF springs, section 5.2.3), very good matching was
368 observed between the identified and the numerically-predicted frequencies. In particular, the
369 average deviation was found in the order of 3-4% for all methods (Table 2, columns 6, 7 and 8).
370 It is interesting to observe that, despite introducing the compliance of the soil, the error between
371 the experimentally- and the numerically-predicted natural frequencies was not substantially
372 increased compared to the negligible 2% average error that was derived for the fixed system.
373 This observation practically implies that the developed finite element models reliably accounted
374 for the compliance of the stabilized soil and successfully predicted the dynamic properties of
375 the bridge-foundation-clay system. This observation also verifies the prediction made regarding
376 the value of G (51 MPa) and ν (0.35). It is noted herein that as the measurement took place
377 during the 14th day of stabilization and the exact hydration phase could not be precisely predicted
378 a lower value of 0.2 was also considered, resulting to an increased error (from 3-4% to 3.2-
379 6.4%).

380 Repeating the comparison for the case of the Hostun sand, higher deviations were naturally
381 observed between the identified and the numerically-predicted frequencies compared to the case

382 of the stabilized soil. Namely, the direct method model (section 5.2.1) presented a 13% average
383 error in the identification of the system's natural frequencies, the intermediate embedded
384 foundation method (section 5.2.2) presented a 10% error and the shallow embedded foundation
385 method (section 5.2.3) presented a 12% error (Table 2, columns 10, 11 and 12). These deviations
386 were associated with the inherent limitations of the above numerical approaches that precisely
387 simulate the soil stiffness of loose and non-cohesive soils, as well as to the complex contact
388 issues between the particular soils and the caisson.

389 It is also interesting to notice that for the soils examined, the identified 3rd and 4th modes of
390 vibration were not closely spaced anymore (46.38 Hz and 56.86 Hz for stabilized soil, 15.99 Hz
391 and 43.25 Hz for Hostun sand); hence, strong correlations (MAC values over 0.90) were
392 observed with the numerical predictions.

393

Conclusions

394 This paper presents the case study of an already constructed, long bridge for which ambient
395 measurements were made available during the construction stage. Based on modal identification
396 at the actual scale and on the ad-hoc designed laboratory experiments at a reduced scale, an
397 effort was made (a) to examine the influence of different soil conditions on the extracted modal
398 parameters of a bridge-foundation-soil system and (b) to compare the efficiencies of alternative
399 numerical approaches in predicting this effect. The conclusions drawn can be summarized as
400 follows:

- 401 • The influence of soil compliance on the dynamic characteristics of a bridge-foundation-
402 soil system was demonstrated by all investigative means (i.e., ambient vibrations,
403 laboratory measurements and numerical results), thus highlighting the necessity of
404 carefully considering soil compliance in the framework of design, assessment and
405 structural health monitoring of bridges. According to the laboratory measurements of the
406 fixed scaled structure, introduction of compliant soil deposits (i.e., stabilized soil and

407 Hostun sand), led to a decrease of all natural frequencies (by 4-30% and 19-76%,
408 respectively). Similarly, the damping ratios of the system were increased for the two
409 soils (by 0.37-3.27% and 1.27-8.59%, respectively) compared to the dynamic
410 characteristics identified for the fixed-base structure.

411 • For stabilized soil conditions, the discrepancies between the identified and the
412 numerically calculated natural frequencies were in the order of 3-4% on average, that is,
413 close to the negligible 2% under fixed boundary conditions. This observation indicates
414 that the developed numerical models predicted reasonably well the dynamic properties
415 of the bridge-foundation-clay system.

416 • The fact that all three herein examined numerical models captured efficiently the
417 stiffness of the bridge-foundation-clay system irrespective of their level of modeling
418 complexity demonstrates that simpler, Winkler-type models are adequately capable of
419 numerically predicting soil stiffness at low computational cost compared to the fully
420 fledged, 3D direct method model, provided that these models are prepared carefully
421 according to the literature and are based on reliable measurements of the soil properties.
422 On the other hand, it is noted that the above assessment is only valid for low amplitude
423 ambient vibrations for which the comparisons were made. Notably, in the case of
424 stronger enforced vibrations (i.e., seismic loading) both soil material and geometric
425 nonlinearities may significantly affect the (instantaneous) natural frequencies in the time
426 domain and as such, the reliability of the examined numerical methods needs to be re-
427 verified.

428 • For the case of Hostun sand soil conditions, more distinct deviations of 10% to 13%
429 were observed between the identified and the numerically calculated natural frequencies.
430 This is primarily attributed to the more extensive nonlinear response that sand materials
431 exhibit even at low levels of strain, and perhaps further to contact issues and ratcheting

432 effects that essentially limit the efficiency of the examined numerical approaches. The
433 above increased numerical error, however, is an indication of equally increased
434 epistemic uncertainty, which should be taken into consideration in the framework of
435 system identification, even at low levels of vibration.

436 **Acknowledgments**

437 The work presented herein was supported by a research grant from the DAAD organization,
438 (Grant No 57055451, Project: DeGrie Lab-Hybrid and Virtual Experimentation for
439 Infrastructures funded by DAAD, Germany). This support is gratefully acknowledged. The
440 authors would like to thank Prof. K. Papadimitriou (University of Thessaly) for making
441 available the measurements of the prototype structure, as well as Prof. G. Manolis (Aristotle
442 University of Thessaloniki) for his scientific input at various stages of this work.

443

444 **References**

445 ABAQUS version 6.12 Computer software]. Pawtucket, RI, Simulia.

446 Allemang, R.J., and Brown D.L. (1982). "A correlation coefficient for modal vector analysis." Proc., 1st
447 International Modal Analysis Conference, SEM, Orlando, Florida, 110–116.

448 Andersen, P., Brincker, R., Peeters, B., De Roeck, G., Hermans, L., and Kramer, C. (1999). "Comparison
449 of system identification methods using ambient bridge test data." Proc., 17th International Modal
450 Analysis Conference, SEM, Kissimmee, Florida, 1, 1035-1041.

451 Antonacci, E., De Stefano, A., Gattulli, V., Lepidi, M., and Matta, E. (2012). "Comparative study of
452 vibration-based parametric identification techniques for a three-dimensional frame structure." Struct.
453 Control Health Monit., 19, 579–608.

454 ASTM Standard D2487. (2011). Standard Practice for Classification of Soils for Engineering Purposes
455 (Unified Soil Classification System), ASTM International, West Conshohocken, Pennsylvania.

456 Bridgman, P.W. (1931). *Dimensional Analysis*, 2nd Edition, Yale University Press, New Haven.

457 Chaudhary, M.T.A., Abe, M., and Fujino, Y. (2001). "Identification of soil-structure interaction effects
458 in base isolated bridges from earthquake records." *Soil Dyn. Earthquake. Eng.*, 21(8), 713–725.

459 Crouse, C.B., Hushmand, B., and Martin, G.R. (1987). "Dynamic soil-structure interaction of single-
460 span bridge." *Earthq. Eng. Struct. Dyn.*, 15(6), 711–729.

461 DIN Standard EN 459-1. (2010). *Building Lime –Part 1 Definitions, specifications and conformity*
462 *criteria*, BEUTH, Berlin, Germany.

463 Dominguez, J., and Roesset, J.M. (1978). *Dynamic stiffness of rectangular foundations*, Research Report,
464 R78-20, MIT.

465 Elsabee, F., and Morray, J.P. (1977). *Dynamic behaviour of embedded foundations*, Research Report,
466 R77-33, MIT.

467 European Standard EN 1998-1. (2004). *Eurocode 8: Design of structures for earthquake resistance - Part*
468 *1: General rules, seismic actions and rules for buildings*, European Committee.

469 Faraonis, P., Sextos, A., Zabel, V., and Wuttke, F. (2014). "Dynamic stiffness of bridge-soil systems
470 based on site and laboratory measurements." *Proc., 2nd International Conference on Bridges Innovations*
471 *on Bridges and Bridge-Soil Interaction*, Eugenides Foundation, Athens, Greece.

472 Finn, W.D.L. (2005). "A study of piles during earthquakes: Issues of design and analysis." *Bull. Earth.*
473 *Eng.*, 3(2), 141-234.

474 Gazetas, G., Dobry, R., and Tassoulas, J. (1985). "Vertical Response of arbitrarily-Shaped Embedded
475 Foundations." *J. Geotech. Eng.*, 111(6), 750-771.

476 Gerolymos, N., and Gazetas, G. (2006). "Development of Winkler model for static and dynamic response
477 of caisson foundations with soil and interface nonlinearities." *Soil Dyn. Earthquake Eng.*, 26(5), 363-

478 376.

479 Kausel, E. (1974). Soil-forced vibrations of circular foundations on layered media, Research Report,
480 R76-06, MIT.

481 Kausel, E., and Ushijima, R. (1979). Vertical and torsional stiffness of circular footings, Research
482 Report, R74-11, MIT.

483 Manos G., Pitiklakis, K., Sextos A., Kourtides, V., Soulis, V., and Thaumpte, J. (2014). "Field
484 experiments for monitoring the dynamic soil–structure–foundation response of a bridge-pier model
485 structure at a test site." *J. of Struct. Eng.*, early view available online.

486 Panetsos, P., Ntotsios, E., Papadimitriou, C., Papadioti, C., and Dakoulas, P. (2010). "Health monitoring
487 of Metsovo bridge using ambient vibrations." *Proc., 5th European Workshop - Structural Health
488 Monitoring*, DEStech, Naples, Italy, 1081-1088.

489 Peeters, B., and De Roeck, G. (1999). "Reference-based stochastic subspace identification for output-
490 only modal analysis." *Mech. Syst. Sig. Process.*, 13(6), 855–878.

491 Peeters, B., and De Roeck, G. (2001). "Stochastic system identification for operational modal analysis:
492 a review." *J. Dyn. Syst. Meas. Control*, 123(4), 659–667.

493 Peeters, B., and Ventura, C. E. (2003). "Comparative study of modal analysis techniques for bridge
494 dynamic." *Mech. Syst. Sig. Process*, 17(5), 965–988.

495 Reynders, E., and De Roeck, G. (2007). "System identification and operational modal analysis with
496 MACEC enhanced." *Proc., 2nd International Operational Modal Analysis Conference*, Department of
497 Civil Engineering Alborg University, Copenhagen, Denmark, 1, 297-304.

498 Reynders, E. (2012). "System identification methods for (Operational) modal analysis: Review and
499 comparison." *Arch. Comput. Methods Eng.*, 19(1), 51–124.

500 Sextos, A. (2014). "ICT applications for new generation Seismic Design, Construction and Assessment
501 of Bridges." *Structural Engineering International*, 24(2), 173-183.

502 Shamsabadi, A., Abazarsa, F., Ghahari, S.F. and Taciroglu, E. (2016). Bridge Instrumentation: Needs,
503 Options, Consequences, in *Developments in International Bridge Engineering Selected Papers from*
504 *Istanbul Bridge Conference 2014*; Alp, C., Gülkan, P., Mahmoud, K. (Eds.), pp. 199-210.

505 Stewart, J.P., and Fenves, G.L. (1998). "System identification for evaluating soil-structure interaction
506 effects in buildings from strong motion recordings." *Earthquake Eng. and Struct. Dynamics*, 27(8), 869-
507 885.

508 Taciroglu, E., Shamsabadi, A., Abazarsa, F., Nigbor, R., and Ghahari, S.F. (2014). "Comparative Study
509 of Model Predictions and Data from the Caltrans-CSMIP Bridge Instrumentation Program: A Case study
510 on the Eureka-Samoa Channel Bridge." Report No. UCLA-SGEL 2014/01, Structural and Geotechnical
511 Engineering Laboratory, University of California, Los Angeles (also Caltrans Report No. CA14-2418).

512 Todorovska, M. (2009.) "Soil-structure identification of Millikan library north-south response during
513 four earthquakes (1970-2002). What caused the observed wandering of the system frequencies." *Bull*
514 *Seismo. Soc. Am.*, 99 (2A), 626-636.

515 Van Overschee P., and De Moor B. (1996). *Subspace identification for linear systems*, Kluwer
516 Academic, Dordrecht.












































517 Varun, Assimaki, D., and Gazetas, G. (2009). "A simplified model for lateral response of large diameter
518 caisson foundations - Linear elastic formulation." *Soil Dyn. Earthquake Eng.*, 29(2), 268-291.

519 Veletsos A.S., and Wei Y.T. (1971). "Lateral and rocking vibrations of footings." *J. Soil Mech. Found.*
520 *Div.*, 97(SM9), 1227-1248.

521 Wolf, J.P. (1989). "Soil-structure interaction analysis in time domain." *Nucl. Eng. Des.*, 111(3), 381-
522 393.

523 Wong H.L., and Luco J.E. (1985). "Tables of impedance functions for square foundations on layered
524 media." *Int. J. Soil Dyn. Earthq. Eng.*, 4(2), 64–81.

1 **Table 1. Section and material properties of studied structures and the developed FE models.**

Characteristics	Prototype			Fixed scaled structure				Scaled structure on stabilized soil (14th day)				Scaled structure on Hostun sand			
	(1)	(2)	(3)	(4)	(5)	(6)	(7)	(8)	(9)	(10)	(11)	(12)			
Structure		Not constructed on site or lab													
Scale	1:1	1:100	Pier height & deck length 1:100	Pier height & deck length 1:100	Pier height, deck length & caisson 1:100	Pier height, deck length & caisson 1:100	Pier height, deck length & caisson 1:100	Pier height, deck length 1:100	Pier height & deck length 1:100	Pier height, deck length & caisson 1:100	Pier height, deck length & caisson 1:100	Pier height, deck length 1:100			
Deck															
Pier															
Caisson			-	-				-				-			
Structure	R/C	R/C	Stainless steel	Stainless steel (E=210GPa)	Stainless steel	Stainless steel (E=210GPa)	Stainless steel (E=210GPa)	Stainless steel (E=210GPa)	Stainless steel	Stainless steel (E=210GPa)	Stainless steel (E=210GPa)	Stainless steel (E=210GPa)			
Soil	Rock (EC8 class A) (EC8 class A)	Rock (EC8 class A)	Fixed	Fixed	Stabilized soil (Vs=166m/sec) (G=51MPa)	3D solid elements (E=51MPa)	6+6 DOF ^a springs (G=51MPa)	6-DOF ^b springs (G=51MPa)	Hostun sand (Vs=59m/sec) (G=4.6MPa)	3D solid elements (G=4.6MPa)	6+6 DOF ^a springs (G=4.6MPa)	6-DOF ^b springs (G=4.6MPa)			
Foundation	R/C caisson	R/C caisson	-	-	R/C caisson (C30/37)	3D solid elements (E=32GPa)	3D solid elements (E=32GPa)	-	R/C caisson (C30/37)	3D solid elements (E=32GPa)	3D solid elements (E=32GPa)	-			

^a Based on the formulas of Kausel 1974, Kausel and Ushijima 1979 and Varun et al. 2009

^b Based on the formulas of Elsabee and Morray 1977 and Gazetas et al. 1985












2

3

4

5

Table 2. Identified and numerically predicted natural frequencies f and damping ratios ζ .

Modes	Prototype structure		Fixed scaled structure				Scaled structure on stabilized soil (14th day)					Scaled structure on Hostun sand			
	(1) Actual structure	(2) Theoretically Scaled	(3) Experiment 1	(4) FEM 1	(5) Experiment 2	(6) FEM 2.1	(7) FEM 2.2	(8) FEM 2.3	(9) Experiment 3	(10) FEM 3.1	(11) FEM 3.2	(12) FEM 3.3			
1-Rotational															
	f (Hz)	f (Hz)	f (Hz)	ζ (%)	f (Hz)	ζ (%)	f (Hz)	ζ (%)	f (Hz)	ζ (%)	f (Hz)	ζ (%)	f (Hz)	ζ (%)	
2-1 st Longit.	0.159	15.90	15.87	0.12	16.02	14.88	0.37	15.18	15.18	15.12	9.60	5.66	11.27	11.31	
3-Transverse	0.305	30.50	23.19	0.10	23.13	19.16	0.85	20.16	20.33	19.54	10.49	5.98	10.81	10.94	
4-2 nd Longit.	0.623	62.30	65.31	0.57	68.23	46.38	1.56	47.07	47.43	41.88	15.99	8.59	18.18	18.24	
5-Bending	0.686	68.60	66.74	0.13	69.71	56.86	3.27	58.50	58.28	54.71	43.25	1.94	41.84	41.97	
Average (%) error ^a	0.908	90.80	88.99	0.55	89.46	85.04	1.81	87.36	87.60	87.59	71.85	1.27	53.50	64.32	
			6.74% ^b		2.12% ^c		2.86% ^d		3.18% ^e		4.02% ^f		12.61% ^g	9.93% ^h	
														11.94% ⁱ	

$$^a \left(\sum_{i=1}^5 \left| \frac{f_{1,i} - f_{2,i}}{f_{1,i}} \right| \right) / 5 \times 100, \text{ where } i^{\text{th}} = \{1, \dots, 5\} \text{ the number of mode}$$

^b f_1 =Theoretically scaled, f_2 = Experiment 1

^c f_1 =Experiment 1, f_2 = FEM 1

^d f_1 =Experiment 2, f_2 = FEM 2.1, ^e f_1 =Experiment 2, f_2 = FEM 2.2, ^f f_1 =Experiment 2, f_2 = FEM 2.3

^g f_1 =Experiment 3, f_2 = FEM 3.1, ^h f_1 =Experiment 3, f_2 = FEM 3.2, ⁱ f_1 =Experiment 23, f_2 = FEM 3.3

7
8
9
10
11
12
13
14

15 **Table 3.** Spring coefficients formulas for the herein developed numerical models (6-DOF model & 12-DOF
 16 model.).

6-DOF model for shallow embedded circular foundation

6 base springs (Elsabee and Morray 1977 and Gazetas et al. 1985)

$$K_{h,x} = K_{h,y} = \frac{8GR}{2-\nu} \left(1 + \frac{1}{2} \frac{R}{H}\right) \quad (5) \quad K_v = \frac{4GR}{1-\nu} \left(1 + 1.28 \frac{R}{H}\right) \quad (6) \quad K_{r,x} = K_{r,y} = \frac{8GR^3}{3(1-\nu)} \left(1 + \frac{1}{6} \frac{R}{H}\right) \quad (7)$$

$$K_t = \frac{16}{3} GR^3 \quad (8)$$

12-DOF model for intermediate embedded circular foundation

6 base springs (Kausel 1979, Kausel and Ushijima 1979)

$$K_{h,x} = K_{h,y} = \frac{8GR}{2-\nu} \left(1 + \frac{1}{2} \frac{R}{H}\right) \left(1 + \frac{2}{3} \frac{D}{R}\right) \left(1 + \frac{5}{4} \frac{D}{H}\right) \quad (9)$$

$$K_v = \frac{4GR}{1-\nu} \left(1 + 1.28 \frac{R}{H}\right) \left(1 + \frac{1}{2} \frac{D}{R}\right) \left(1 + 0.85 - 0.28 \frac{D}{R} \frac{D/H}{1-D/H}\right) \quad (10)$$

$$K_{r,x} = K_{r,y} = \frac{8GR^3}{3(1-\nu)} \left(1 + \frac{1}{6} \frac{R}{H}\right) \left(1 + 2 \frac{D}{R}\right) \left(1 + 0.7 \frac{D}{H}\right) \quad (11) \quad K_t = \frac{16}{3} GR^3 \left(1 + 2.67 \frac{D}{R}\right) \quad (12)$$

springs middle of foundation height (Varun et al. 2009)

$$K_{h,x} = K_{h,y} = 1.828 \left(\frac{D}{B}\right)^{-0.15} ED \quad (13)$$

$$K_v = Eq.(10) - Eq.(6) \quad (14)$$

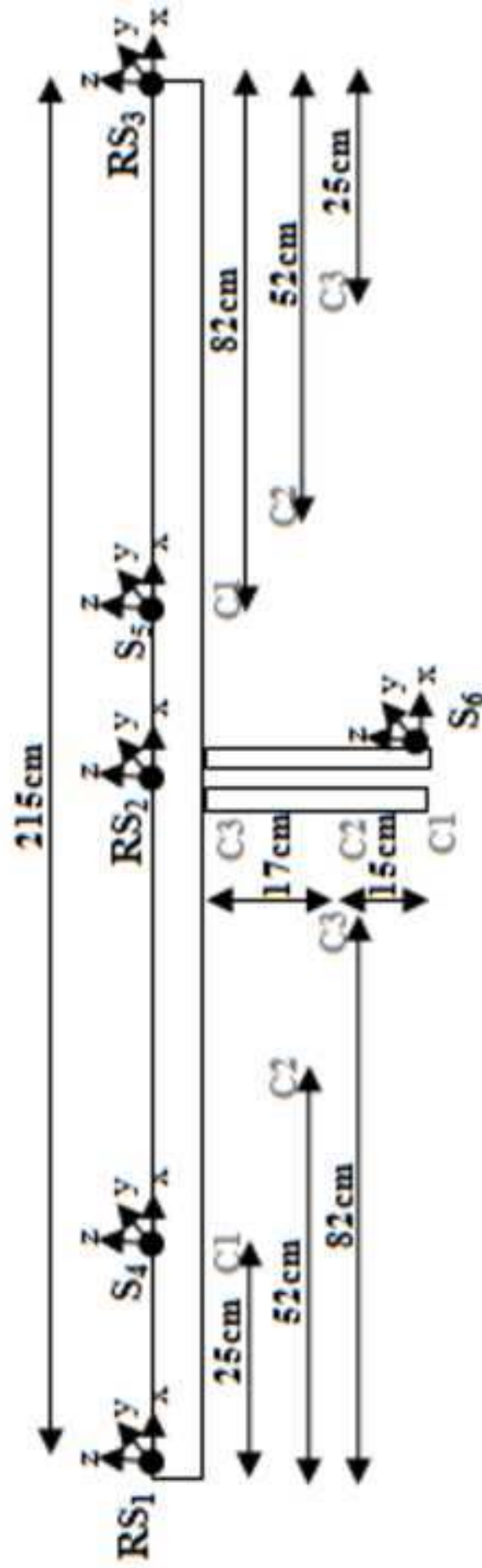
$$K_{r,x} = K_{r,y} = (1.06 + 0.227 \frac{D}{B}) ED^2 D \quad (15)$$

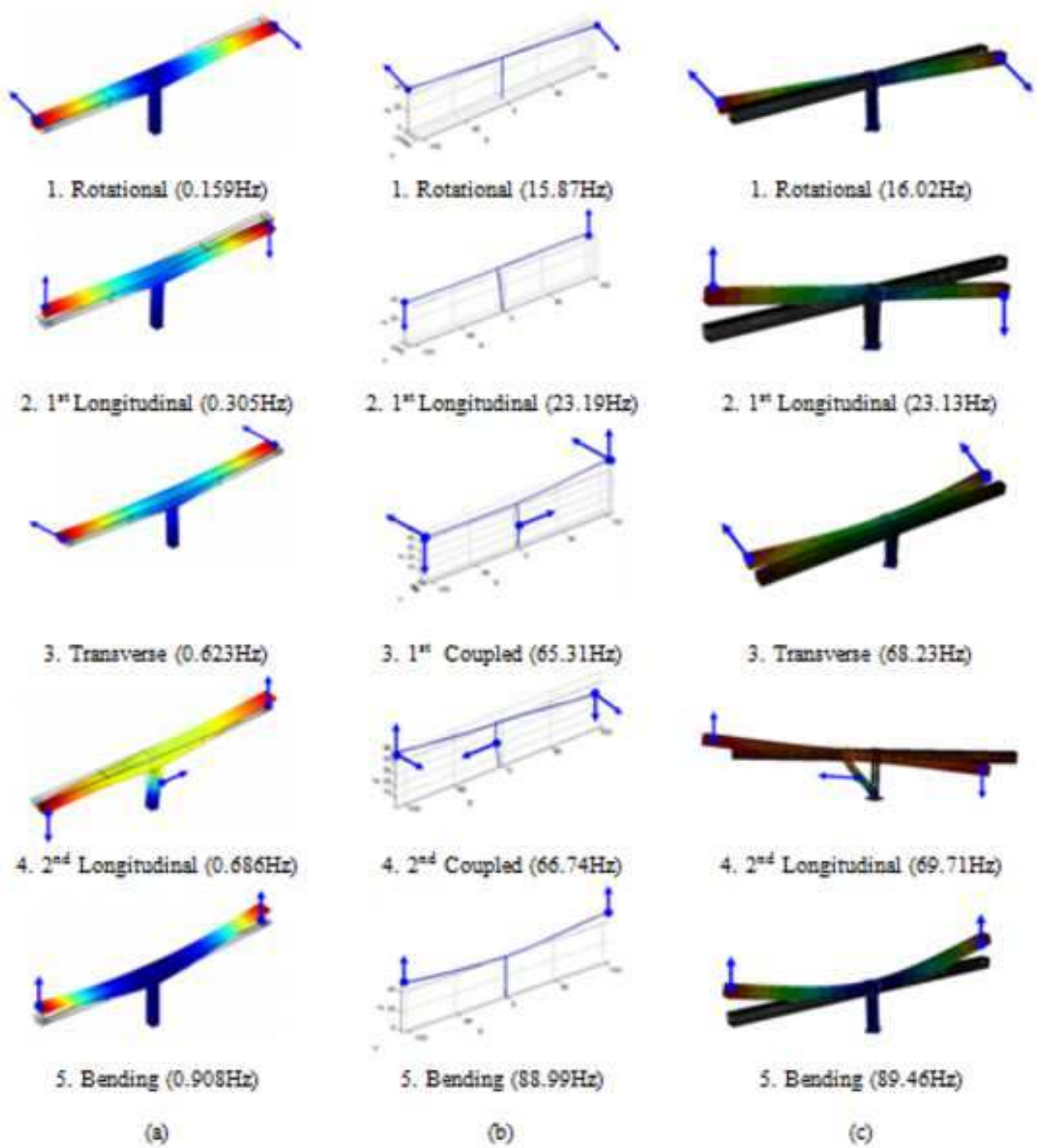
$$K_t = Eq.(12) - Eq.(8) \quad (16)$$

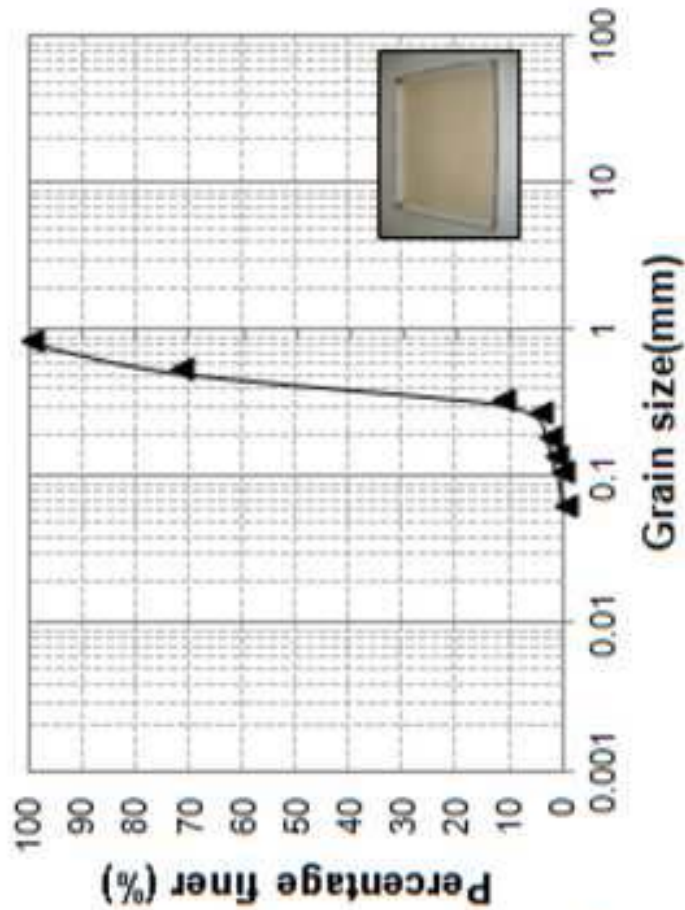
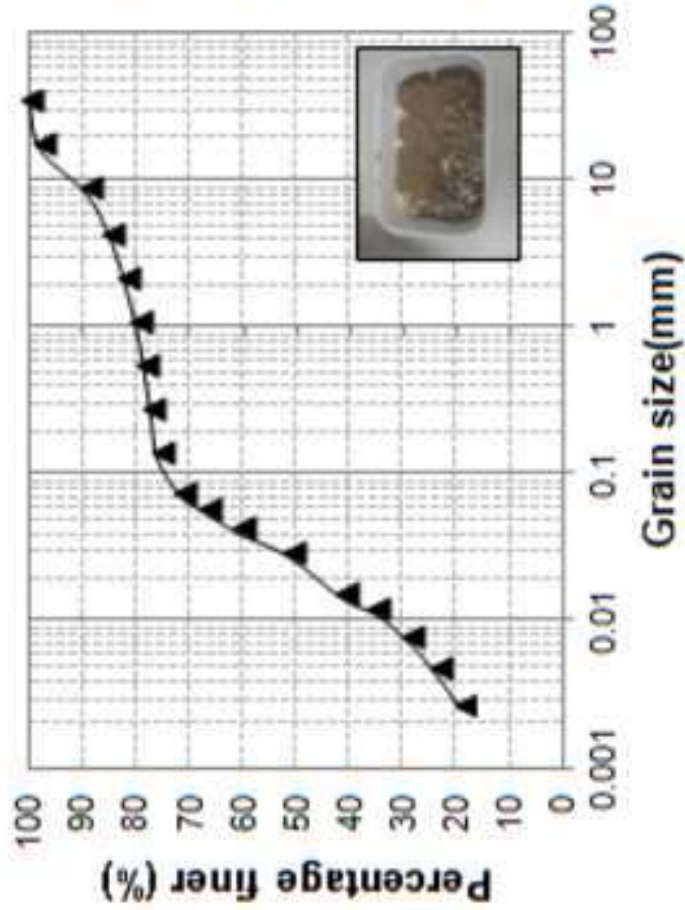
G=shear modulus, E=Young's modulus of Elasticity, ν =Poisson's ratio, R=foundation radius, H=height of soil stratum, D=foundation height, B=foundation diameter













(a)



(b)



(c)



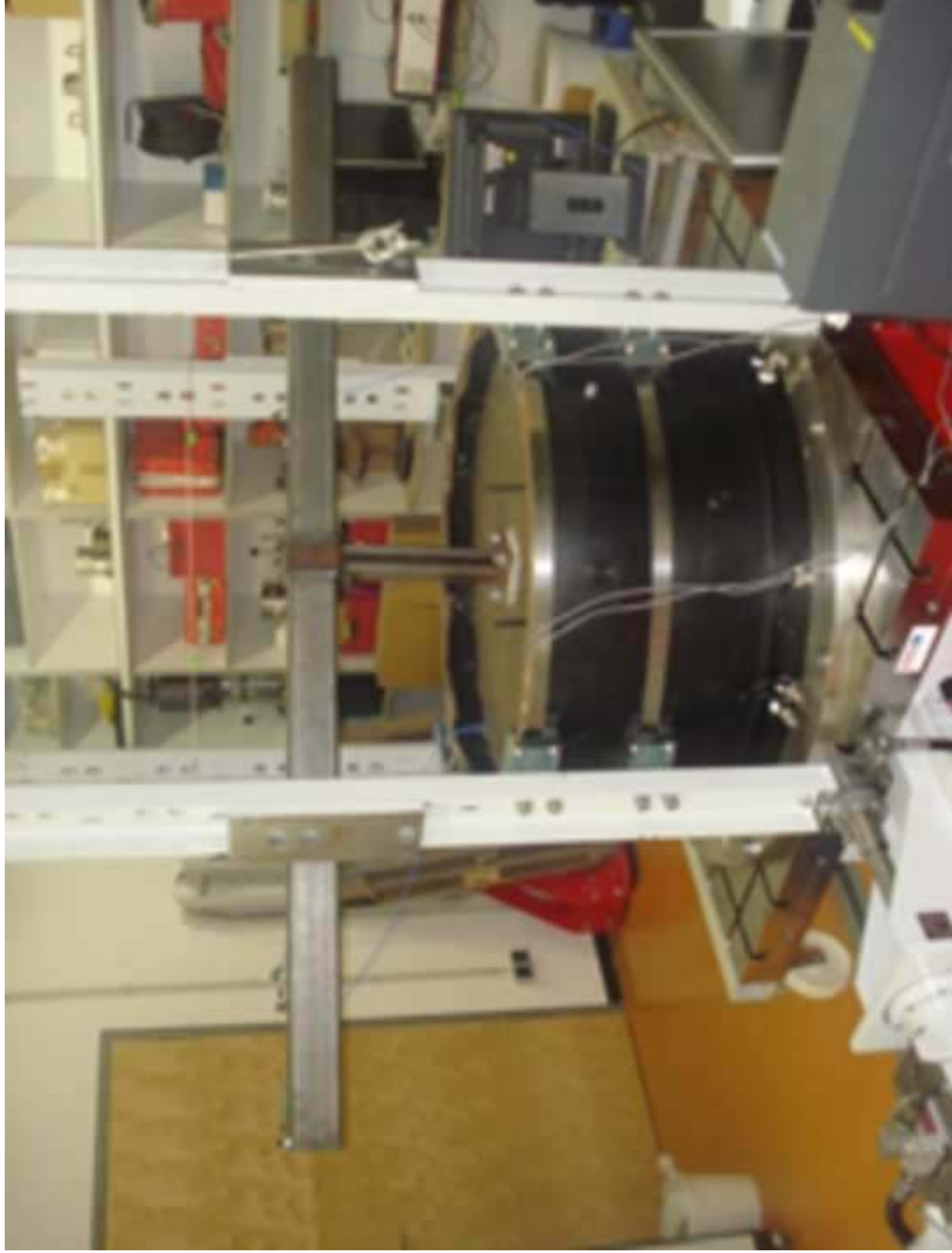
(d)

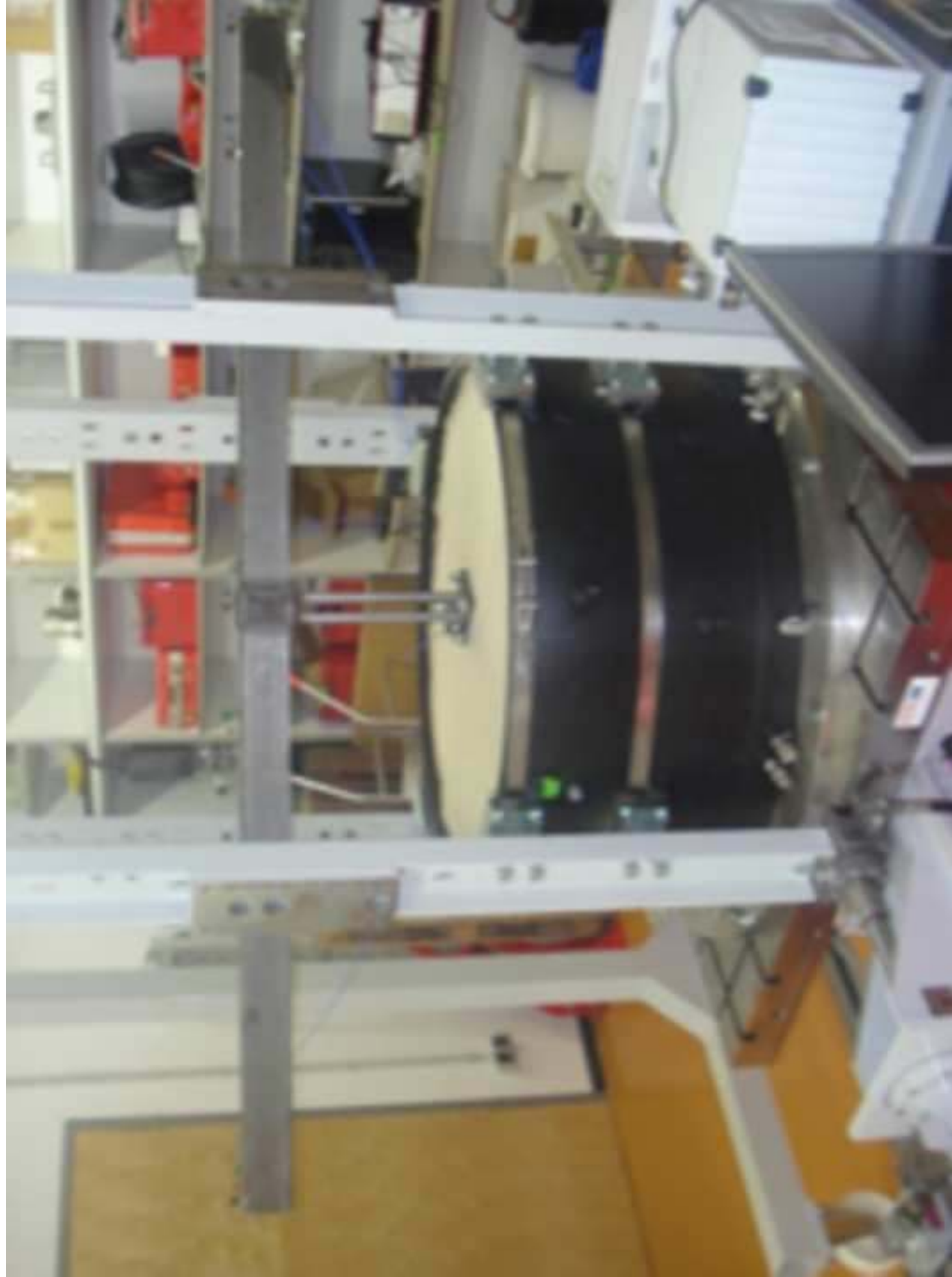


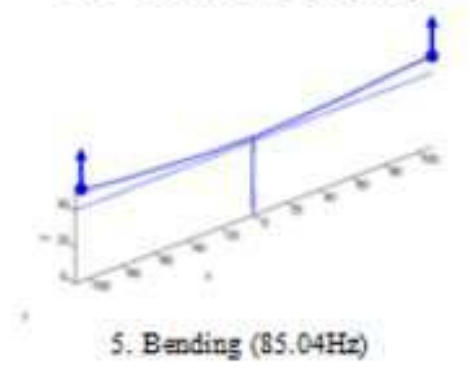
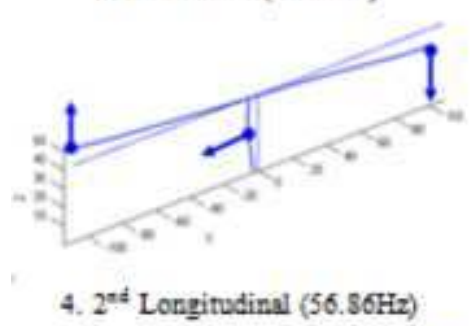
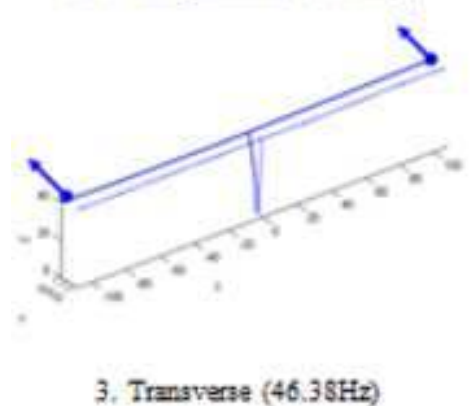
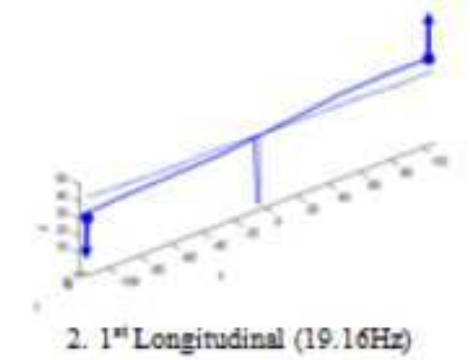
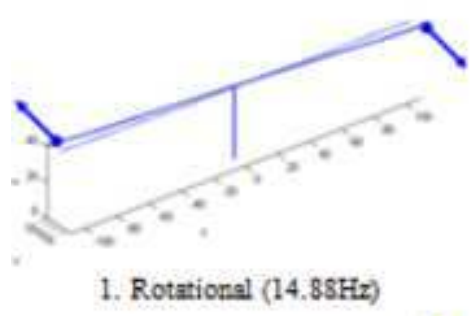
(e)



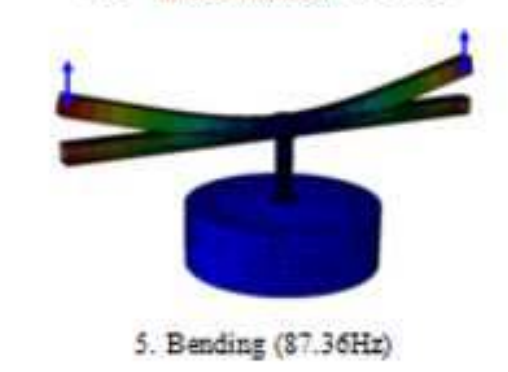
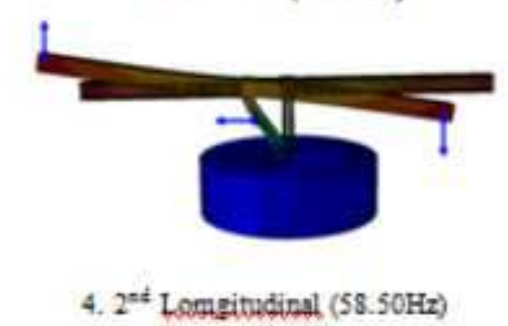
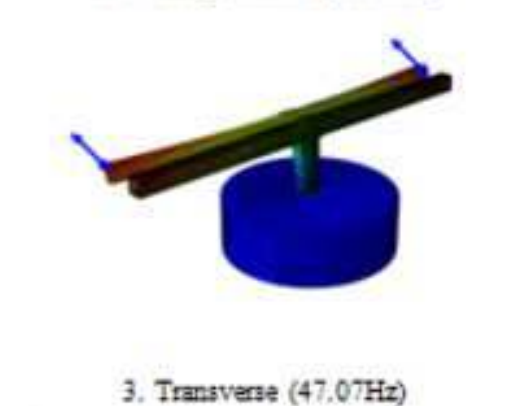
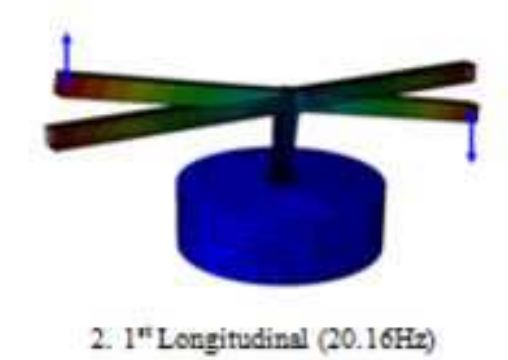
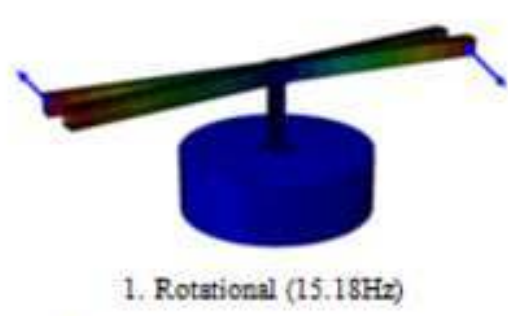
(f)



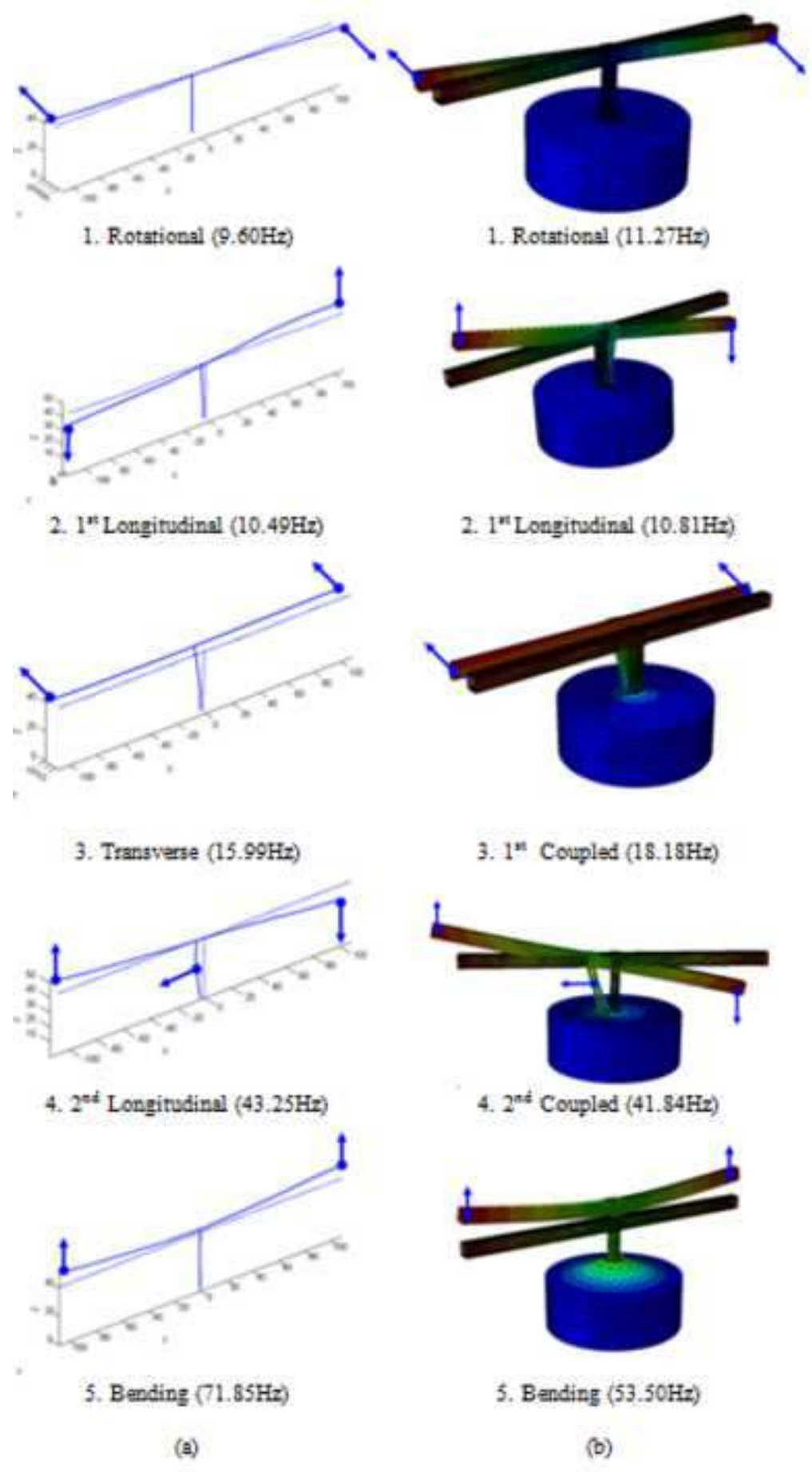


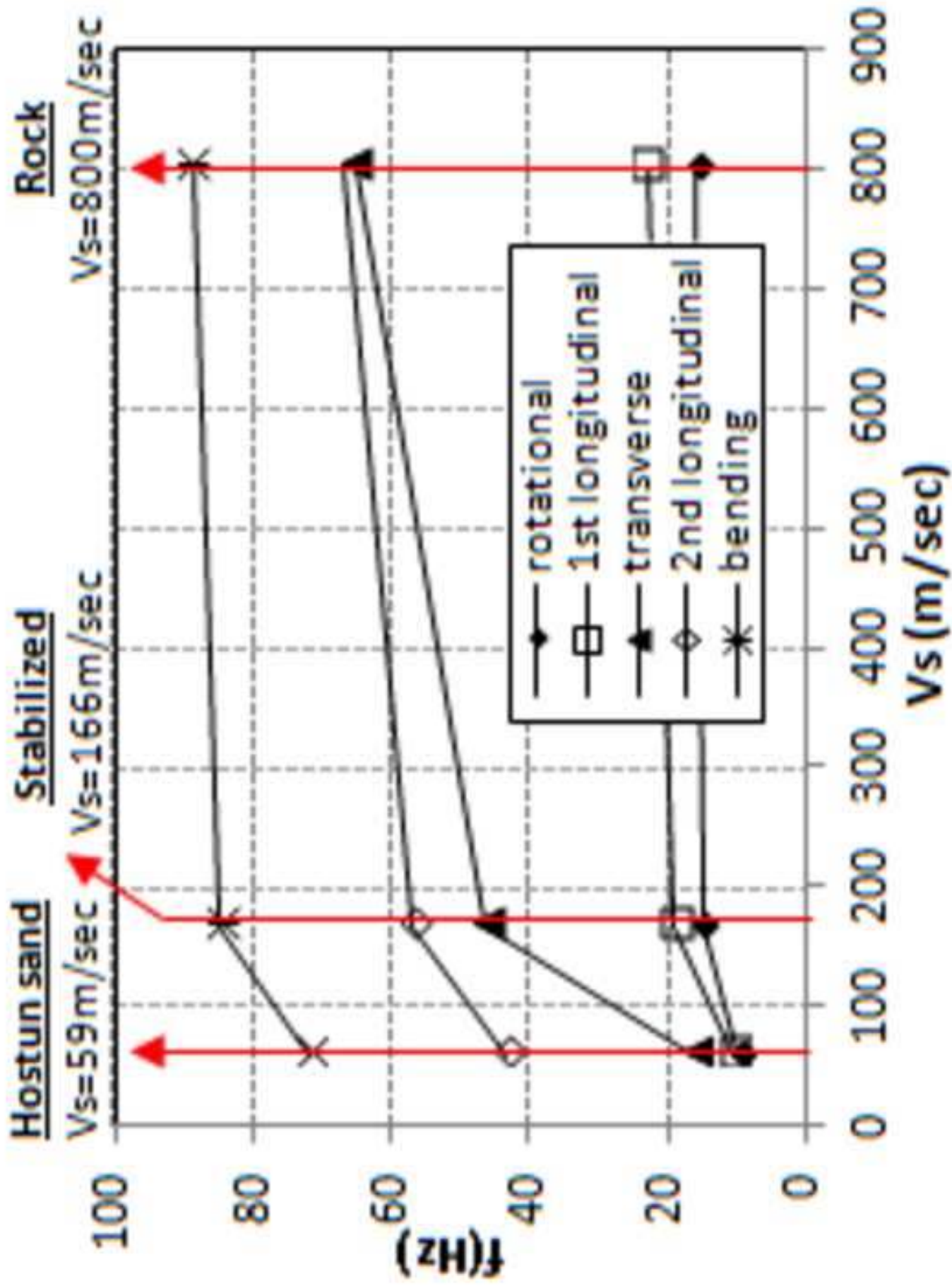


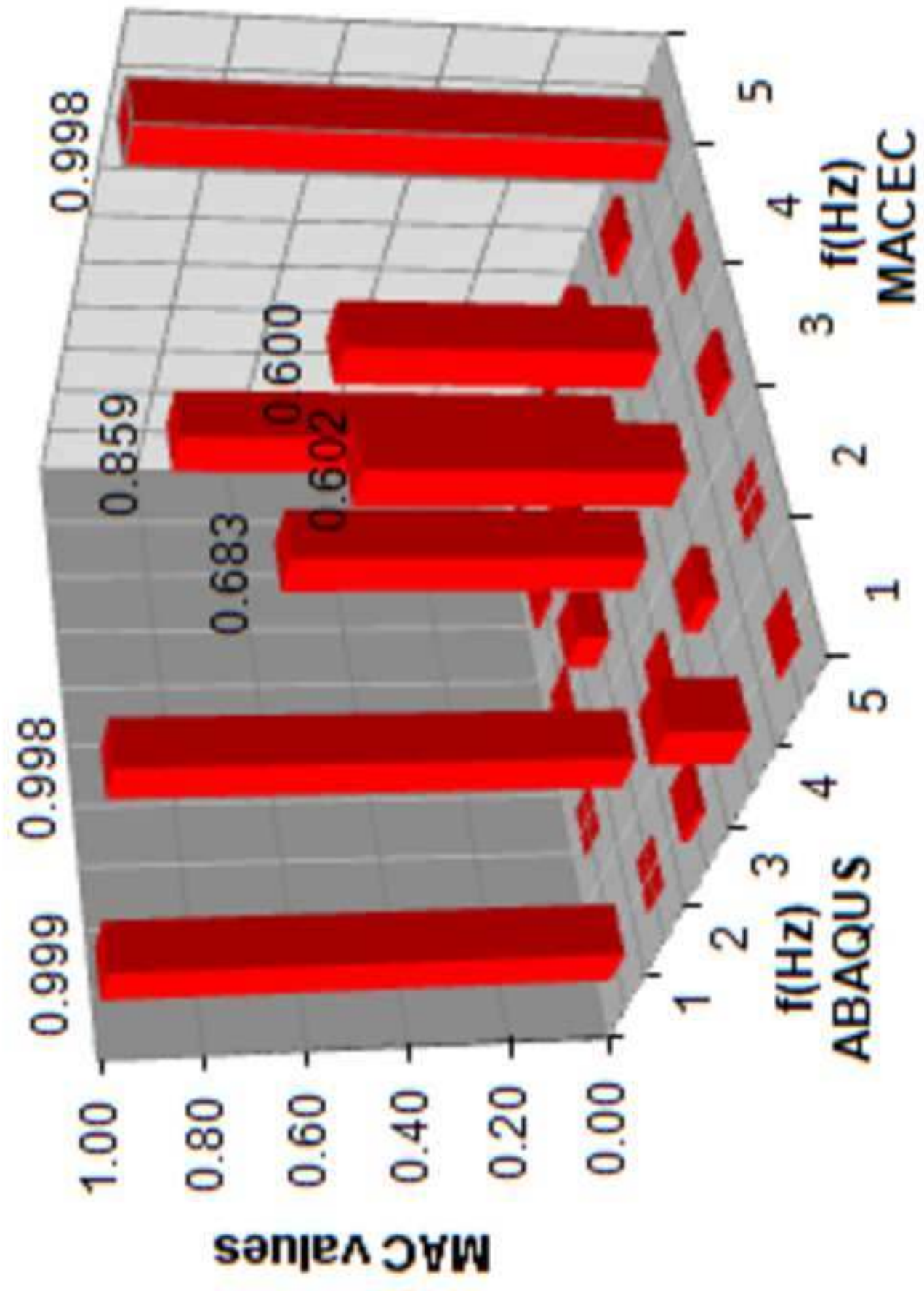
(a)



(b)







- 1 **Fig. 1.** Metsovo Bridge segments during the construction stage.
- 2 **Fig. 2.** Fixed scaled structure equivalent of Metsovo Bridge M3 pier-deck tested at the laboratory.
- 3 **Fig. 3.** First arrangement (set up 1) of accelerometers and alternative positions of sensors S_4 , S_5 and S_6
4 for the two alternative arrangements (set up 2 and set up 3).
- 5 **Fig. 4.** (a) Numerical mode shapes of the full scale model (Panetsos et al 2009, identified
6 mode shapes of the full scale model also available in Panetsos et al 2009), (b) identified mode
7 shapes of the fixed scaled model and (c) numerically predicted mode shapes of the fixed
8 scaled model.
- 9 **Fig. 5.** Grain size distribution curve for the stabilized soil (left curve, before stabilization) and the
10 Hostun sand (right curve).
- 11 **Fig. 6.** Construction stages of stabilized soil:(a) laboratory box fixed on the shaking table before soil
12 placement, (b) mixture of the 1st soil layer with water at a mixture apparatus, (c) injection of lime to
13 the mix of soil with water, (d) placement of the 1st layer of stabilized soil inside the laboratory box
14 and compaction until it reached 5cm height, (e) formation of a rough surface with the use of a knife to
15 enhance cohesion between the 1st and the 2nd soil layer and (f) embedment of the 15cm concrete
16 foundation in the last 3 layers of the overall 30cm high (6 layers of 5cm) stabilized soil.
- 17 **Fig. 7.** Scaled structure on stabilized soil.
- 18 **Fig. 8.** Scaled structure on Hostun sand.
- 19 **Fig. 9.** (a) Identified and (b) numerically predicted mode shapes of the scaled structure on stabilized
20 soil.
- 21 **Fig. 10.** (a) Identified and (b) numerically predicted mode shapes of the scaled structure on
22 the Hostun sand.

23 **Fig. 11.** Influence of Hostun sand ($V_s=59\text{m/s}$), stabilized soil ($V_s=166\text{m/s}$) and rock ($V_s=800\text{m/s}$) on
24 the identified modes of the equivalent superstructure of the Metsovo M_3 cantilever.

25 **Fig. 12.** Calculated values of the Modal Assurance Criterion (MAC) between the identified (MACEC)
26 and numerically predicted (ABAQUS) mode shapes, for the case of fixed boundary conditions.

ASCE Authorship, Originality, and Copyright Transfer Agreement

Publication Title: Soil-bridge system stiffness identification through field and laboratory measurements

Manuscript Title: Soil-bridge system stiffness identification through field and laboratory measurements

Author(s) – Names, postal addresses, and e-mail addresses of all authors

Anastasios Sextos, University of Bristol, Civil Engineering Department, BS8 1TR, Bristol, UK, asextos@bristol.ac.uk

Periklis Faraonis, Aristotle University of Thessaloniki, Civil Engineering Department, 54124, Thessaloniki, Greece, pfaraonis@civil.auth.gr

Volkmar Zabel, Marienstrasse 15, 99423 Weimar, Germany, volkmar.zabel@uni-weimar.de

Frank Wuttke, Ludewig-Meyn Street 10, 24118 Kiel, Germany, fw@gpi.uni-kiel.de

Tobias Arndt, Coudraystrasse 11c, 99423 Weimar, Germany, tobias.arndt@uni-weimar.de, Panagioti

I. Authorship Responsibility

To protect the integrity of authorship, only people who have significantly contributed to the research or project and manuscript preparation shall be listed as coauthors. The corresponding author attests to the fact that anyone named as a coauthor has seen the final version of the manuscript and has agreed to its submission for publication. Deceased persons who meet the criteria for coauthorship shall be included, with a footnote reporting date of death. No fictitious name shall be given as an author or coauthor. An author who submits a manuscript for publication accepts responsibility for having properly included all, and only, qualified coauthors.

I, the corresponding author, confirm that the authors listed on the manuscript are aware of their authorship status and qualify to be authors on the manuscript according to the guidelines above.

Anastasios Sextos

Print Name

Signature



THE 21 OCT 2014

Date

II. Originality of Content

ASCE respects the copyright ownership of other publishers. ASCE requires authors to obtain permission from the copyright holder to reproduce any material that (1) they did not create themselves and/or (2) has been previously published, to include the authors' own work for which copyright was transferred to an entity other than ASCE. Each author has a responsibility to identify materials that require permission by including a citation in the figure or table caption or in extracted text. Materials re-used from an open access repository or in the public domain must still include a citation and URL, if applicable. At the time of submission, authors must provide verification that the copyright owner will permit re-use by a commercial publisher in print and electronic forms with worldwide distribution. For Conference Proceeding manuscripts submitted through the ASCE online submission system, authors are asked to verify that they have permission to re-use content where applicable. Written permissions are not required at submission but must be provided to ASCE if requested. Regardless of acceptance, no manuscript or part of a manuscript will be published by ASCE without proper verification of all necessary permissions to re-use. ASCE accepts no responsibility for verifying permissions provided by the author. Any breach of copyright will result in retraction of the published manuscript.

I, the corresponding author, confirm that all of the content, figures (drawings, charts, photographs, etc.), and tables in the submitted work are either original work created by the authors listed on the manuscript or work for which permission to re-use has been obtained from the creator. For any figures, tables, or text blocks exceeding 100 words from a journal article or 500 words from a book, written permission from the copyright holder has been obtained and supplied with the submission.

Anastasios Sextos

Print name

Signature



THE 21 OCT 2014

Date

III. Copyright Transfer

ASCE requires that authors or their agents assign copyright to ASCE for all original content published by ASCE. The author(s) warrant(s) that the above-cited manuscript is the original work of the author(s) and has never been published in its present form.

The undersigned, with the consent of all authors, hereby transfers, to the extent that there is copyright to be transferred, the exclusive copyright interest in the above-cited manuscript (subsequently called the "work") in this and all subsequent editions of the work (to include closures and errata), and in derivatives, translations, or ancillaries, in English and in foreign translations, in all formats and media of expression now known or later developed, including electronic, to the American Society of Civil Engineers subject to the following:

- The undersigned author and all coauthors retain the right to revise, adapt, prepare derivative works, present orally, or distribute the work, provided that all such use is for the personal noncommercial benefit of the author(s) and is consistent with any prior contractual agreement between the undersigned and/or coauthors and their employer(s).
- No proprietary right other than copyright is claimed by ASCE.
- If the manuscript is not accepted for publication by ASCE or is withdrawn by the author prior to publication (online or in print), or if the author opts for open-access publishing during production (journals only), this transfer will be null and void.
- Authors may post a PDF of the ASCE-published version of their work on their employers' **Intranet** with password protection. The following statement must appear with the work: "This material may be downloaded for personal use only. Any other use requires prior permission of the American Society of Civil Engineers."
- Authors may post the **final draft** of their work on open, unrestricted Internet sites or deposit it in an institutional repository when the draft contains a link to the published version at www.ascelibrary.org. "Final draft" means the version submitted to ASCE after peer review and prior to copyediting or other ASCE production activities; it does not include the copyedited version, the page proof, a PDF, or full-text HTML of the published version.

Exceptions to the Copyright Transfer policy exist in the following circumstances. Check the appropriate box below to indicate whether you are claiming an exception:

U.S. GOVERNMENT EMPLOYEES: Work prepared by U.S. Government employees in their official capacities is not subject to copyright in the United States. Such authors must place their work in the public domain, meaning that it can be freely copied, republished, or redistributed. In order for the work to be placed in the public domain, ALL AUTHORS must be official U.S. Government employees. If at least one author is not a U.S. Government employee, copyright must be transferred to ASCE by that author.

CROWN GOVERNMENT COPYRIGHT: Whereby a work is prepared by officers of the Crown Government in their official capacities, the Crown Government reserves its own copyright under national law. If ALL AUTHORS on the manuscript are Crown Government employees, copyright cannot be transferred to ASCE; however, ASCE is given the following nonexclusive rights: (1) to use, print, and/or publish in any language and any format, print and electronic, the above-mentioned work or any part thereof, provided that the name of the author and the Crown Government affiliation is clearly indicated; (2) to grant the same rights to others to print or publish the work; and (3) to collect royalty fees. ALL AUTHORS must be official Crown Government employees in order to claim this exemption in its entirety. If at least one author is not a Crown Government employee, copyright must be transferred to ASCE by that author.

WORK-FOR-HIRE: Privately employed authors who have prepared works in their official capacity as employees must also transfer copyright to ASCE; however, their employer retains the rights to revise, adapt, prepare derivative works, publish, reprint, reproduce, and distribute the work provided that such use is for the promotion of its business enterprise and does not imply the endorsement of ASCE. In this instance, an authorized agent from the authors' employer must sign the form below.

U.S. GOVERNMENT CONTRACTORS: Work prepared by authors under a contract for the U.S. Government (e.g., U.S. Government labs) may or may not be subject to copyright transfer. Authors must refer to their contractor agreement. For works that qualify as U.S. Government works by a contractor, ASCE acknowledges that the U.S. Government retains a nonexclusive, paid-up, irrevocable, worldwide license to publish or reproduce this work for U.S. Government purposes only. This policy DOES NOT apply to work created with U.S. Government grants.

I, the corresponding author, acting with consent of all authors listed on the manuscript, hereby transfer copyright or claim exemption to transfer copyright of the work as indicated above to the American Society of Civil Engineers.

Anastasios Sextos

Print Name of Author or Agent

AT 2010 FEB 10

Signature of Author of Agent



THE FEDERAL

Date

More information regarding the policies of ASCE can be found at <http://www.asce.org/authorsandeditors>

ASCE Worksheet for Sizing Technical Papers & Notes

Please complete and save this form then email it with each manuscript submission.

Note: The worksheet is designed to automatically calculate the total number of printed pages when published in ASCE tw format.

Journal Name:	Journal of structural engineering	Manuscript # (if known):	
Author Full Name:		Author Email:	

The maximum length of a technical paper is 10,000 words and word-equivalents or 8 printed pages. A technical note should not exceed 3,500 word-equivalents in length or 4 printed pages. Approximate the length by using the form below to calculate the total number of words in the text to the total number of word-equivalents of the figures and tables to obtain a grand total of words for the paper/note to fit ASCE format. Over must be approved by the editor; however, valuable overlength contributions are not intended to be discouraged by this procedure.

1. Estimating Length of Text

A. Fill in the four numbers (highlighted in green) in the column to the right to obtain the total length of text.

NOTE: Equations take up a lot of space. Most computer programs don't count the amount of space around display equations. Plan on counting 3 lines of text for every simple equation (single line) and 5 lines for every complicated equation (numerator and denominator).

Estimating Length of Text	
Count # of words in 3 lines of text:	37
Divided by 3	3
Average # of words per line	12
Count # of text lines per page	24
# of words per page	296.00
Count # of pages (don't add references & abstract)	17.4
Title & Abstract	500
Total # refs	35
Length of Text is	848
	6498
	498
	6996
	6

2. Estimating Length of Tables

A. First count the longest line in each column across adding two characters between each column and one character between each word to obtain total characters.

1-column table = up to 60 characters wide	2-column table = 61 to 120 characters wide
---	--

B. Then count the number of text lines (include footnote & titles)

1-column table = up to 60 characters wide by: 17 lines (or less) = 158 word equiv. up to 34 lines = 315 word equiv. up to 51 lines = 473 word equiv. up to 68 text lines = 630 word equiv.	2-column table = 61 to 120 characters wide by: 17 lines (or less) = 315 word equiv. up to 34 lines = 630 word equiv. up to 51 lines = 945 word equiv. up to 68 text lines = 1260 word equiv.
---	---

C. Total Characters wide by Total Text lines = word equiv. as shown in the table above. **Add word equivalents** for each table in the column labeled "Word Equivalents."

3. Estimating Length of Figures

A. First reduce the figures to final size for publication.

Figure type size can't be smaller than 6 point (2mm).

B. Use ruler and measure figure to fit 1 or 2 column wide format.

1-column fig. = up to 3.5 in.(88.9mm)	2-col. fig. = 3.5 to 7 in.(88.9 to 177.8 mm) wide
---------------------------------------	---

C. Then use a ruler to check the height of each figure (including title & caption).

1-column fig. = up to 3.5 in.(88.9mm) wide by: up to 2.5 in.(63.5mm) high = 158 word equiv. up to 5 in.(127mm) high = 315 word equiv. up to 7 in.(177.8mm) high = 473 word equiv. up to 9 in.(228.6mm) high = 630 word equiv.	2-column fig. = 3.5 to 7 in.(88.9 to 177.8 mm) wide by: up to 2.5 in.(63.5mm) high = 315 word equiv. up to 5 in.(127mm) high = 630 word equiv. up to 7 in.(177.8mm) high = 945 word equiv. up to 9 in.(228.6mm) high = 1260 word equiv.
--	--

D. Total Characters wide by Total Text lines = word equiv. as shown in the table above. **Add word equivalents** for each table in the column labeled "Word Equivalents."

Total Tables/Figures:	5201
Total Words of Text:	6996

(word equivalents)

Total words and word equivalents:	12197
printed pages:	10

Estimating Length of Tables & Figures		
Tables	Word Equivalents	Figures
Table 1	630	Figure 1
2	630	2
3	315	3
4	0	4
5	0	5
6	0	6
7	0	7
8	0	8
9	0	9
10	0	10
11	0	11
12	0	12
13	0	13
14	0	14
15	0	15
Please double-up tables/figures if additional space is needed (ex. 20+21).		16
		17
		18
		19
		20 and 21

two-column

words and
:t and adding
:length papers

subtotal
plus headings
TOTAL words
printed pages

Figures:
Word Equivalents
158
158
315
630
630
630
315
158
158
158
158
158
0
0
0
0
0
0
0
0
0
0



DEPARTMENT OF CIVIL ENGINEERING
Queen's Building, University Walk
Bristol BS8 1TR, UK
Tel: (0) 7751 679688
Email: a.sextos@bristol.ac.uk

December 11th, 2015

To the Associate Editor of the
ASCE Journal of Bridge Engineering,

Subject: Manuscript BEENG-2173R3 – Revision for Editor Only

Re.: “Soil-bridge system stiffness identification through field and laboratory measurements” by
A. Sextos, P. Faraonis, V. Zabel, F. Wuttke, T. Arndt & P. Panetsos

We would like to thank all Reviewers for accepting our manuscript and the Associate Editor for his willingness to check few additional clarifications requested by the XX Reviewer (herein addressed in lines 103-108).

Can we once again thank the Associate Editor for handling the Review process in an excellent manner.

Yours sincerely,

A handwritten signature in blue ink, appearing to be "AS", with a long horizontal flourish extending to the right.

Dr Anastasios Sextos, MASCE, Associate Professor

On behalf of the co-authors